RSC Advances

PAPER

Check for updates

Reversible ammonia uptake at room temperature in a robust and tunable metal–organic framework†

Jaechul Lee, ‡[a] Younggyu Seo, ‡[a] Dong Won Kang, [b] Seungjae Park, [a] Hyunyong Kim, [a] Jaheon Kim, [c] Kimoon Kim, [ade] Chang Seop Hong, *[b] Dae-Woon Lim*[fg] and Eunsung Lee *[ad]

Ammonia is useful for the production of fertilizers and chemicals for modern technology, but its high toxicity and corrosiveness are harmful to the environment and human health. Here, we report the recyclable and tunable ammonia adsorption using a robust imidazolium-based MOF (JCM-1) that uptakes 5.7 mmol g^{-1} of NH$_3$ at 298 K reversibly without structural deformation. Furthermore, a simple substitution of NO$_3^-$ with Cl$^-$ in a post-synthetic manner leads to an increase in the NH$_3$ uptake capacity of JCM-1(Cl$^-$) up to 7.2 mmol g^{-1}.

Introduction

Ammonia is one of the essential chemicals not only for fertilizers in agriculture but also for various industrial applications such as an alternative fuel, refrigerants, and a precursor for numerous nitrogenous compounds. As the second most-produced chemical in the world, over 150 million tons of ammonia is annually produced.[1] Such a huge production and extensive usage of NH$_3$ raises concerns about the environment and human health issues because of its toxic and corrosive properties. The United States Department of Labor alerts that exposure only to a small amount of ammonia can damage a human body. In the atmosphere, NH$_3$ can combine with sulfate and nitrate to form fine particulate matter (PM2.5), causing severe particulate air pollution.[2–4] In this context, practical methods and materials for the removal of ammonia emitted in the air are highly desirable.

[a] *Department of Chemistry, Pohang University of Science and Technology (POSTECH), Pohang, 37673, Republic of Korea. E-mail: eslee@postech.ac.kr*

[b] *Department of Chemistry, Korea University, Seoul 02841, Republic of Korea. E-mail: cshong@korea.ac.kr*

[c] *Department of Chemistry, Soongsil University, Seoul 06978, Republic of Korea*

[d] *Division of Advanced Materials Science, Pohang University of Science and Technology, Pohang 37673, Republic of Korea*

[e] *Center for Self-assembly and Complexity, Institute for Basic Science (IBS), Pohang, 37673, Republic of Korea*

[f] *Department of Chemistry, Graduate School of Science, Kyoto University, Kitashirakawa Oiwakecho, Sakyo-ku, Kyoto 606-8502, Japan*

[g] *Department of Chemistry and Medical Chemistry, Yonsei University, Wonju, 26493, Republic of Korea. E-mail: limdaewoon@yonsei.ac.kr*

† Electronic supplementary information (ESI) available. CCDC 1912377. For ESI and crystallographic data in CIF or other electronic format see DOI: 10.1039/d2ra01270g

‡ These authors contribute equally.

Metal–organic frameworks (MOFs) have emerged as a promising material for the capture of toxic chemicals such as NH$_3$,[5–19] NO$_x$,[20–23] SO$_x$,[24–26] and volatile organic compounds[27,28] because well-ordered porosity with feasible chemical and structural tunability of pore surfaces enables such applications. Synthesis of MOFs with high structural stability toward corrosive species is a critical issue for real-world applications. In this regard, several MOFs that can take up NH$_3$ under atmospheric condition has been developed recently.[5–19,29] Nevertheless, structural instability of adsorbent and high regeneration temperature are still remaining challenges for practical applications.[5,7–19] MOFs showing recyclable ammonia adsorption while retaining its porosity are still very rare. The limited stability of MOFs under ammonia conditions is ascribed to the coordinating nature of NH$_3$. That is, NH$_3$ as a good sigma donating ligand can replace the existing ligand in MOFs, leading to framework decomposition.[30] Next, strong NH$_3$···MOF interactions through open metal sites or acid–base interactions necessitate high regeneration temperature, which in turn needs high thermal stability of MOFs and energy-intensive regeneration processes as well. Thus far, MFM-300(Al) reported by M. Schröder and co-workers in 2018 is a representative MOF that can repeatedly adsorb ammonia with regeneration at room temperature.[29] In addition, there have been reported numerous examples for uptaking ammonia using MOFs for the past five years (Table S3†). Nevertheless, it is still challenging to devise robust MOFs that enables reversible uptake of ammonia under mild regeneration conditions.

Recently, we reported a microporous MOF, JCM-1 ([Co(PzIm)(NO$_3$)], H$_2$PzIm = 1,3-bis(3,5-dimethyl-1*H*-pyrazol-4-yl)-imidazolium).[31] JCM-1 has a cationic three-dimensional framework formed by Co(II)–pyrazolate coordination bonds, where imidazolium groups are aligned along the channels containing NO$_3^-$ ions (Fig. S1†). Since azolates such as

pyrazolate, imidazolate, and triazolate have a greater Lewis basicity than common carboxylates, MOFs constructed from azolate linkers are well-known to possess superior durability against polar solvent.[32–34] Indeed, **JCM-1** has outstanding properties such as high hydrolytic stability, a unique pore structure, and gas separation abilities.[31] For its unique gas sorption properties, the imidazolium functionality in **JCM-1** plays a crucial role as a mimic of ionic liquid solutions. We also found that some imidazolium-based ionic liquids show high ammonia solubility by weak hydrogen bonds between imidazolium salt and NH_3.[35–38] Studies on the NH_3 adsorption using imidazolium-based MOFs have not been reported so far, which motivated us to investigate the NH_3 capture ability of **JCM-1** (Fig. 1).

Results and discussion

Synthesis and characterization of JCM-1 and JCM-1(Cl⁻)

Herein, we report the recyclable and tunable ammonia adsorption using **JCM-1**, which is the first demonstration of NH_3 capture utilizing an imidazolium-based MOF. **JCM-1** was synthesized according to the previous procedure by heating a mixture of $Co(NO_3)_2(H_2O)_6$ and the $H_2PzImCl$ ligand in N,N-dimethylformamide (details in the ESI†). In the single-crystal X-ray structure of **JCM-1**, one-dimensional channels are running through the [001] direction with an aperture size of 12.5×3.9 Å. The nitrate anion in the channels of **JCM-1** can be fully replaced by chloride ion to obtain **JCM-1(Cl⁻)** by post-synthetic anion exchange method following the previous procedures. The crystal structure of **JCM-1(Cl⁻)** by single-crystal X-ray diffraction analysis showed that the space group of **JCM-1(Cl⁻)** was not changed ($I4_1/amd$) with almost the same unit cell parameters as **JCM-1** (Fig. S2 and Table S1†); the cationic scaffold remained unchanged, and only the anion species in the pore was replaced after ion substitution. When the crystals of **JCM-1** were treated with 1 M ammonia solution in THF for 24 hours (Fig. 2a), the crystals remained intact, which secures the chemical stability of **JCM-1** toward corrosive ammonia, enabling NH_3 gas uptake measurements.

The total NH_3 uptake amounts of **JCM-1** at 1 bar were 7.9 and 5.7 mmol g^{-1} at 273 K and 298 K, respectively (Fig. 2b), which are comparable with other NH_3 adsorbing MOFs.[5–19,29] Notably, **JCM-1** surpasses other materials in terms of framework stability upon regeneration, which are the critical properties of energy-
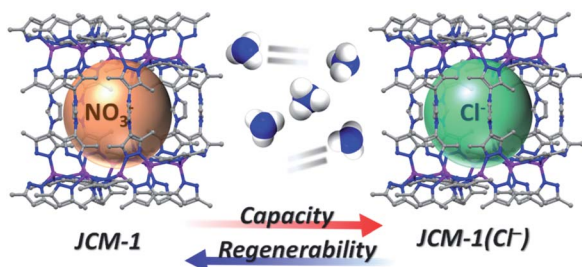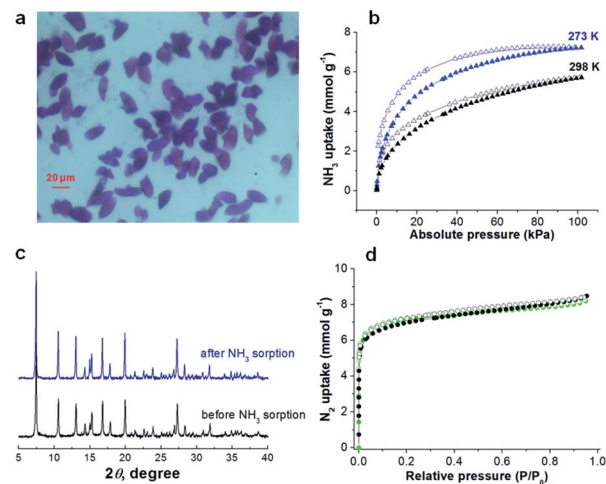

Fig. 2 (a) A picture for the crystals of **JCM-1** stored in 1 M ammonia THF solution at room temperature for 24 hours. (b) NH_3 adsorption isotherms of **JCM-1** at 273 K and 298 K. (c) PXRD patterns and (d) N_2 adsorption isotherms of **JCM-1** before and after ammonia adsorption experiments (black circle, before NH_3 sorption; light-green circle, after NH_3 sorption).

efficient NH_3 adsorbent materials. Although a substantial number of MOFs were tested for ammonia adsorption thus far, they suffer from structural deformation after exposure to corrosive NH_3 gas.[5,7–19,39,41] Many of the MOFs show decreased porosity with the degradation of crystallinity during repeated NH_3 adsorption–desorption processes, resulting in peak broadening in powder X-ray diffraction (PXRD) patterns. In contrast, **JCM-1** could maintain the initial crystallinity and the porosity after NH_3 adsorption experiments, which was confirmed by the almost unchanged PXRD patterns and N_2 sorption isotherms (Fig. 2c and d).

Ammonia adsorption of JCM-1 and JCM-1(Cl⁻)

Unlike other MOFs capturing ammonia, **JCM-1** has no open metal sites and no acid functional groups for strong interaction with NH_3. Instead, it possesses imidazolium functional groups on the pore surfaces to form weak hydrogen bonds with NH_3.
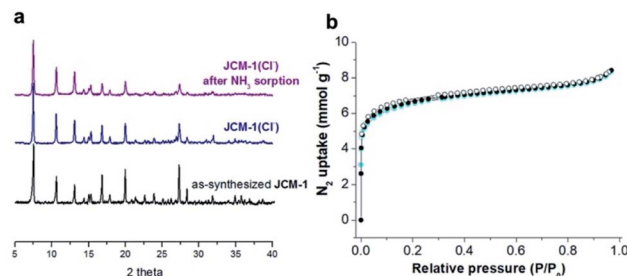

Fig. 1 Schematic illustration of ammonia adsorption with **JCM-1** and **JCM-1(Cl⁻)**.

Fig. 3 (a) PXRD patterns of as-synthesized **JCM-1**, **JCM-1(Cl⁻)** before NH_3 adsorption, and **JCM-1(Cl⁻)** after NH_3 adsorption experiment. (b) N_2 adsorption isotherms of **JCM-1(Cl⁻)** before and after ammonia adsorption experiments (black circle: before NH_3 sorption, cyan circle: after NH_3 sorption).

The imidazolium protons and counter anions in **JCM-1** can act respectively as a proton donor and a proton acceptor, enabling cooperative hydrogen bonding with NH_3. This weak but effective intermolecular interaction seems to facilitate the reactivation of **JCM-1** after repeated NH_3 adsorption measurements. We carried out cycle experiments (Fig. 4a and c), and observed that the sample could be fully evacuated at room temperature under dynamic vacuum. The NH_3 uptake capacity was well retained over five cycles, showing the facile regenerability of **JCM-1** under mild conditions.

The NH_3 uptake capacity and sorption affinity of **JCM-1** could be also modulated by replacing NO_3^- with Cl^- in a postsynthetic manner, where **JCM-1** was soaked in a methanol solution of LiCl for a week to give anion-exchanged **JCM-1(Cl⁻)**. Although the effectiveness of anion inserted into a MOF for modulating ammonia uptake was reported by Binaeian,[15] the exchange of counter anions in the cationic framework was investigated for ammonia uptake in our case. The NH_3 uptake capacity of **JCM-1(Cl⁻)** was increased, although its N_2 adsorption behavior was almost the same (Fig. 3). Because of high porosity of **JCM-1** and the weaker interaction with nitrogen compared to ammonia, the anion exchange effect on the nitrogen adsorption properties of **JCM-1** and **JCM-1(Cl⁻)** is less pronounced compared to the ammonia adsorption. At 1 bar, **JCM-1(Cl⁻)** adsorbed 11.7 and 7.2 mmol g^{-1} of NH_3 at 273 K and 298 K, respectively, which increased by 48% (273 K) and 26% (298 K), compared with **JCM-1** (Fig. 5). The crystallinity and porosity of **JCM-1(Cl⁻)** were well retained after NH_3 adsorption, as confirmed by PXRD and N_2 adsorption data (Fig. 3). In the cycling experiment, **JCM-1(Cl⁻)** showed gradually decreasing NH_3 capacity after the first cycle (Fig. 4b and d), which means that the sample was not fully activated at room temperature. Activation of the sample after the 5th cycle at an elevated
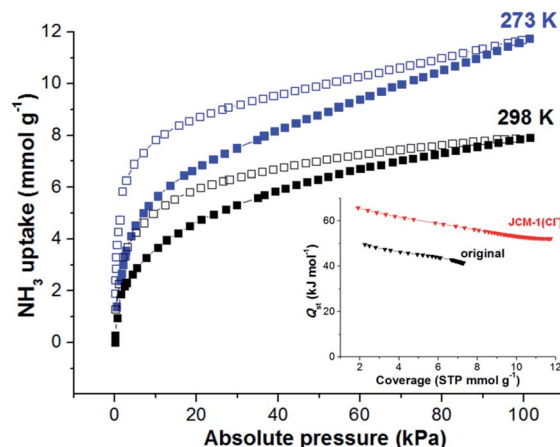

Fig. 5 NH_3 adsorption isotherms of **JCM-1(Cl⁻)** at 273 K and 298 K. Inset: isosteric heat of sorption (Q_{st}) of NH_3 in **JCM-1** and **JCM-1(Cl⁻)**.

temperature of 358 K for 5 h regenerated **JCM-1(Cl⁻)** and the initial NH_3 uptake capacity of was almost recovered (Fig. 4d).

The isosteric heats (Q_{st}) of adsorption for NH_3 within **JCM-1** or **JCM-1(Cl⁻)** was calculated by employing the Virial method.[41] Because of the hysteresis in the NH_3 adsorption isotherms, we calculated the Q_{st} values using the desorption curves, which is also valid for explaining the change in the regeneration temperatures.[42–44] The Q_{st} values for NH_3 desorption in **JCM-1(Cl⁻)** were higher by *ca.* 20 kJ mol^{-1} than **JCM-1** in all coverages (inset in Fig. 5). The higher Q_{st} value of **JCM-1(Cl⁻)** supports the reason for the increased regeneration temperature after ion substitution. The enhanced NH_3 affinity of **JCM-1(Cl⁻)** could be confirmed using density functional theory (DFT) calculations. For DFT calculations, the appropriate structural models of each framework were prepared using the crystal structures of **JCM-1** and **JCM-1(Cl⁻)**. The initial coordinate of NH_3 was loaded into each model structure, followed by further geometry optimization (see the ESI†). The NH_3 molecule showed stronger interaction with the imidazolium-Cl^- pair than the imidazolium-NO_3^- in the optimized structures, as the interaction enthalpies of **JCM-1** and **JCM-1(Cl⁻)** with NH_3 molecule were calculated to be 20.8 kJ mol^{-1} and 50.0 kJ mol^{-1}, respectively (Fig. S3 and S4†), which is qualitatively following the experimental observations.

Mechanism of ammonia adsorption on JCM-1 and JCM-1(Cl⁻)

A simple interpretation of the above observation is that the adsorbed NH_3 molecule interacts more strongly with Cl^- than NO_3^- ions. Contrary to this expectation, DFT calculations revealed a more delicate interplay between NH_3 and the imidazolium–anion pairs. Before NH_3 loading, NO_3^- or Cl^- is engaged in hydrogen bonding with the imidazolium in the framework. The distance between NO_3^- and imidazolium proton is 1.93 Å, whereas the distance between Cl^- and imidazolium proton is 2.21 Å (Fig. S5†). Upon adsorption, NH_3 molecules have to compete with the anions to form hydrogen bonding with the imidazolium proton. As expected, in the optimized structures of the NH_3-loaded **JCM-1** and **JCM-1(Cl⁻)**,
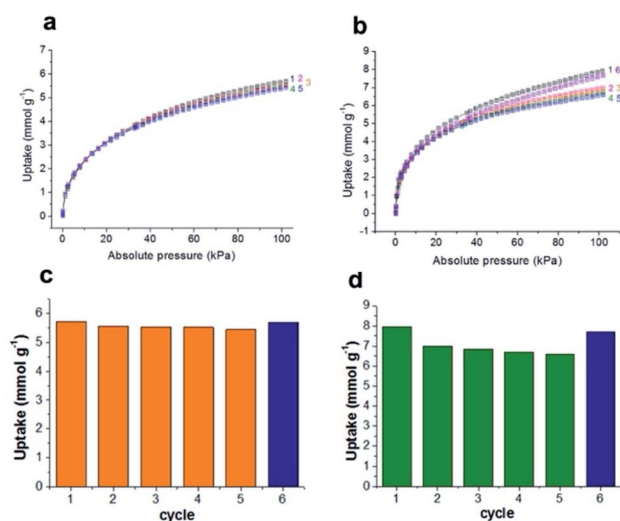

Fig. 4 Adsorption isotherms of (a) repeated NH_3 adsorption cycles in **JCM-1** and (b) **JCM-1(Cl⁻)** at ambient conditions (298 K and 1 bar) uptake capacity of (c) repeated NH_3 adsorption cycles in **JCM-1** and (d) **JCM-1(Cl⁻)** at ambient conditions (298 K and 1 bar).
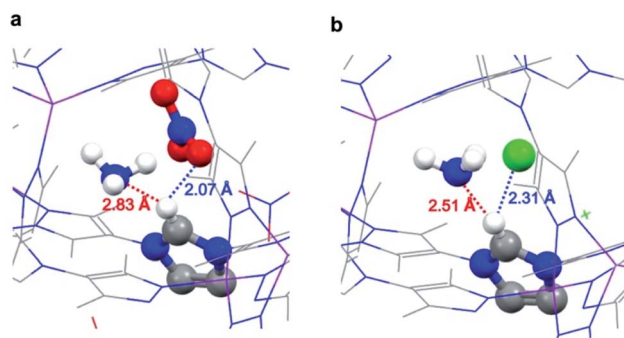
Fig. 6 NH$_3$-loaded optimized structures of (a) **JCM-1** and (b) **JCM-1(Cl$^-$)**.

the distances between the anion and imidazolium proton increased (Fig. 5). On the other hand, a weak hydrogen bond between an NH$_3$ molecule and the imidazolium proton was detected. In the NH$_3$@**JCM-1**, the distance between the nitrogen atom of NH$_3$ and the imidazolium proton was 2.83 Å (Fig. 6a). Interestingly, in the NH$_3$@**JCM-1(Cl$^-$)**, the distance was 2.51 Å, which is significantly shorter than that of **JCM-1** and explains why **JCM-1(Cl$^-$)** exhibits the enhanced NH$_3$ affinity (Fig. 6b). As above mentioned, this interaction is similar to that for imidazolium-based ionic liquids having high ammonia solubility.[35–38]

The interaction between NH$_3$ and the imidazolium group on the pore surface was experimentally observed by IR spectroscopy (Fig. S6†). We measured the IR spectra of the frameworks before and after exposure to NH$_3$ gas. In both structures, imidazolium C–H stretching bands[45] (2900–3100 cm^{-1}) were slightly broadened and blue-shifted after exposure to the NH$_3$ atmosphere.[40,46] The band-broadening and band-shift are indicative of the formation of the weak hydrogen bond between imidazolium and the NH$_3$ molecule, which is coincident with the DFT calculation results.

Dynamic breakthrough curves were obtained under dry and humid conditions (0% relative humidity (RH) and 80% RH) at a feed concentration of 1000 ppm NH$_3$ and a temperature of 298 K. We observed the increase in the adsorption amount of ammonia in **JCM-1(Cl$^-$)** in both humid and wet conditions, which shows the same tendency with the adsorption isotherms, while **JCM-1** adsorbs only dry ammonia (Fig. S7–S10†).

Conclusions

In conclusion, we report **JCM-1** which can adsorb a high amount of NH$_3$ at an ambient condition without structural deformation. **JCM-1** is recyclable even at room temperature through the weak interaction between NH$_3$ and imidazolium functionalities by mimicking ionic liquids. Furthermore, we demonstrated the control of the NH$_3$ sorption property of **JCM-1** by simple ion substitution in a post-synthetic manner. After exchanging the anion from nitrate to chloride, the affinity of MOF toward NH$_3$ was enhanced resulting in the increase in the uptake capacity while the regenerability was slightly decreased.

This work suggests a new potential application of imidazolium-based MOFs for ammonia capture, as well as the effect of the anion species for ammonia adsorption in ionic porous materials.

Experimental

Materials and methods

All the reagents and solvents were commercially available and used as supplied without further purification. Elemental analysis (EA) for C, H, and N were carried out using Flash 2000 (Thermo Fisher Scientific Inc.). FT-IR measurements were processed in Bruker ALPHA FT-IR spectrometer. Single crystal X-ray diffraction (SXRD) analysis was carried out at synchrotron radiation of 2D-SMC and 6D-C&S UNIST-PAL (crystallography) at the Pohang Accelerator Laboratory (PAL, Korea). The powder XRD diffraction patterns were obtained on a Rigaku Smartlab system equipped with Cu sealed tube. Thermogravimetric analysis (TGA) were measured under N$_2$ atmosphere with a PerkinElmer Pyris. All gas sorption isotherms were measured with BELSORP-max volumetric adsorption equipment. Purified compounds were further dried under high vacuum (0.01–0.05 Torr).

MOF synthesis

JCM-1 ([Co(PzIm)(NO$_3$)], H$_2$PzIm = 1,3-bis(3,5-dimethyl-1*H*-pyrazol-4-yl)-1*H*-imidazol-3-ium) and **JCM-1(Cl$^-$)** ([Co(PzIm)(Cl)]) was synthesized following our previously reported methods.[31]

Synthesis of JCM-1. Co(NO$_3$)$_2$·6H$_2$O (0.075 mmol, 21.9 mg) and H$_2$PzImCl (0.025 mmol, 7.3 mg) were dissolved in 0.5 mL of DMF in a 4 mL vial. The vial was stand in an oven at 120 °C for 3 days to yield purple single crystals. The crystals were washed with water and DMF several times, followed by solvent exchange to methanol. Then, the crystals were activated under high vacuum at 393 K to afford **JCM-1** ([Co(PzIm)(NO$_3$)]). Elemental analysis data: anal. calcd for (C$_{13}$H$_{15}$CoN$_7$O$_3$)(H$_2$O)$_{3.5}$: C, 35.54; H, 5.05; N, 22.32. Found: C, 35.31; H, 4.87; N, 22.32.

Synthesis of JCM-1(Cl$^-$). The as-synthesized **JCM-1** powder was shaken in methanolic solution of 1 M LiCl. The solution was exchanged once a day for a week, followed by washing with fresh methanol to afford the product **JCM-1(Cl$^-$)**. It is noteworthy that the exchange process was carried out longer (7 days) than before (3 days) for the full ion substitution. After anion exchange, the product was washed with fresh methanol several times and dried under high vacuum at 373 K. In addition to the previously reported FT-IR, PXRD and EDS analysis, the fully exchanged product was further confirmed by elemental analysis and single-crystal XRD analysis. Elemental analysis data of **JCM-1(Cl$^-$)**: anal. calcd for (C$_{13}$H$_{15}$CoN$_6$)Cl$_1$(H$_2$O)$_2$: C, 40.48; H, 4.97; N, 21.79. Found: C, 40.15; H, 5.28; N, 21.61.

X-ray crystallographic analysis

Single crystal X-ray diffraction (SXRD) analysis was carried out at the synchrotron radiation of 2D-SMC at the Pohang Accelerator Laboratory (PAL, Korea). The SXRD patterns of crystals

coated with paratone oil were collected at 100 K. Using Olex2,[47] the structures were solved by ShelXT[48] using Intrinsic Phasing. The crystal structure of **JCM-1(Cl⁻)** was refined by ShelXL[49] using least squares minimization. CCDC 1912377 contains the structural information for **JCM-1(Cl⁻)**.

Gas sorption experiments

Repeated NH₃ sorption using JCM-1. The activation/adsorption cycle was repeated over five times. Between each cycle, samples were activated at room temperature for 10 hours under dynamic vacuum. The NH₃ uptake patterns were well retained with negligible decrease in uptake capacity. The initial NH₃ adsorption capacity was fully restored after activating at a higher temperature.

Repeated NH₃ sorption using JCM-1(Cl⁻). The activation/adsorption cycle of **JCM-1(Cl⁻)** was repeated over five times. Between each cycle, samples were activated at room temperature under dynamic vacuum for 10 h. The NH₃ uptake capacity was decreased after the 1st cycle, which means the NH₃ was not fully detached from the framework. Interestingly, in the rest of the cycle, the adsorption capacity was no longer significantly decreased. When regenerated at a higher temperature, the initial NH₃ adsorption capacity was recovered. It means that the capacity decrease in the cycle experiment was due to the enhanced affinity of the framework with NH₃ gas, not due to the collapse of the framework.

Isosteric heat of sorption

The isosteric heat of sorption Q_{st} was calculated using the virial type expression to fit the isotherms of 273 K and 298 K.[50]

$$\ln P = \ln N + 1/T \sum_{i=0}^{m} a_i N^i + \sum_{i=0}^{n} b_i N^i$$

where P is the pressure of the gas phase at equilibrium (bar), N is the adsorbed amount per mass of adsorbent (mmol g⁻¹), T is the absolute temperature, a_i and b_i are virial coefficients, and m and n are numbers of coefficients used to describe the isotherms.

$$Q_{st} = -R \sum_{i=0}^{m} a_i N^i$$

Then, with the virial coefficient (a_i) and the following equation, the coverage-dependent isosteric heat of sorption was calculated. R is the universal gas constant.

DFT calculations

Both geometry optimizations and frequency calculations were performed using Gaussian 09 using B3LYP/6-31G(d,p) basis set.[51] In the geometry optimization, the default tight convergence in the SCF cycle was used without any orbital symmetry constraints. For the calculation of MOFs, model structures were generated with appropriate pore structure based on crystallography data. Two-layer ONIOM method[52] was used with B3LYP/6-31G(d,p) basis set for high level, and molecular mechanics using UFF force field[53] for low level. Coordinates of the rigid

cationic framework of MOF structures (**JCM-1** and **JCM-1(Cl⁻)**) were fixed according to the crystallography data, while the geometry of anions (NO₃⁻ or Cl⁻) and ammonia molecule were optimized during the calculation. High level model systems in ONIOM calculation were selected as one imidazolium and its counter anions (NO₃⁻ or Cl⁻) with an ammonia molecule. The interaction enthalpies of the framework with the guest molecule were calculated from the difference in total energies for the model structure ($H_{interaction} = H_{MOF} + H_{guest} - H_{MOF\ with\ guest}$).

Breakthrough experiments

Breakthrough experiments were carried out with a BELCAT-II equipped with a BELMASS mass spectrometer. The pelletized sample was packed in the breakthrough column of 0.5 cm in width and 1.0 cm in height and activated at 120 °C for 10 h in a He flow. The dry ammonia breakthrough experiments were performed in 1000 ppm NH₃ gas balanced with He at 25 °C. In the case of wet ammonia breakthrough experiments, the sample was pre-saturated with humid (80% RH) He gas for 5 h at 25 °C prior to each measurement. And then, 1000 ppm NH₃ gas balanced with humid (80% RH) He was introduced to the sample-packed column for 18 h at 25 °C. The regeneration between consecutive ammonia breakthrough cycles was different to the degassing procedure. The sample was activated with 25 °C for 10 h in a He flow. The effluent gas signal was continuously monitored by the BELMASS mass spectrometer. The amount of adsorbed NH₃ was calculated by the integration of the breakthrough curve with ChemMaster program. The total gas flow was set at 30 sccm in all cases.

In the case of dry ammonia breakthrough experiments, the amount of adsorbed ammonia in the breakthrough curve was calculated through the ChemMaster program by integrating the hatched area which is the gap between the elute curves of the saturated ammonia in the blank and the sample. The weight of glass beads in blank test (or the weight of the sample in breakthrough curve) was measured by comparing empty column weight and weight of column with beads (or sample) after activation. The calibration factor (count per mmol) of dry 1000 ppm breakthrough test was calculated with the ChemMaster program by choosing the flat region of blank test after NH₃ fully was eluted.

In the case of wet ammonia breakthrough experiments, the ammonia breakthrough curves after pre-humidification for 5 h were depicted. The amount of adsorbed ammonia in the breakthrough curve at 80% RH and 1000 ppm was calculated by the ChemMaster program by integrating the hatched area which is the gap between the elute curves of saturated ammonia in the blank and the sample. The weight of glass beads in the blank test (or the weight of the sample in the breakthrough) was measured by comparing empty column weight and weight of column with beads (or sample) after activation. The calibration factor (count per mmol) of the breakthrough test at 80% RH and 1000 ppm was calculated by choosing the flat region of the blank test after NH₃ was fully eluted. It should be noted that the ammonia breakthrough curve at dry 1000 ppm and that at 80% RH and 1000 ppm were not compatible in retention time

because two have distinct blank breakthrough curves and so the calibration factors.

Conflicts of interest

There are no conflicts to declare.

Acknowledgements

Notes and references

1 *NITROGEN (FIXED)—ammonia*, U.S. Geological Survey, Mineral Commodity Summaries, 2018, pp. 116–117, https://minerals.usgs.gov/minerals/pubs/commodity/nitrogen/mcs-2018-nitro.pdf.

2 M. Sharma, S. Kishore, S. N. Tripathi and S. N. Behera, *J. Atmos. Chem.*, 2007, **58**, 1–17.

3 L. Gong, R. Lewicki, R. J. Griffin, F. K. Tittel, C. R. Lonsdale, R. G. Stevens, J. R. Pierce, Q. G. J. Malloy, S. A. Travis, L. M. Bobmanuel, B. L. Lefer and J. H. Flynn, *Atmos. Environ.*, 2013, **77**, 893–900.

4 Y. Wu, B. Gu, J. W. Erisman, S. Reis, Y. Fang, X. Lu and X. Zhang, *Environ. Pollut.*, 2016, **218**, 86–94.

5 D. Britt, D. Tranchemontagne and O. M. Yaghi, *Proc. Natl. Acad. Sci. U. S. A.*, 2008, **105**, 11623–11627.

6 O. T. Wilcox, A. Fateeva, A. P. Katsoulidis, M. W. Smith, C. A. Stone and M. J. Rosseinsky, *Chem. Commun.*, 2015, **51**, 14989–14991.

7 M. J. Katz, A. J. Howarth, P. Z. Moghadam, J. B. DeCoste, R. Q. Snurr, J. T. Hupp and O. K. Farha, *Dalton Trans.*, 2016, **45**, 4150–4153.

8 Y. Chen, X. Zhang, K. Ma, Z. Chen, X. Wang, J. Knapp, S. Alayoglu, F. Wang, Q. Xia, Z. Li, T. Islamoglu and O. K. Farha, *ACS Appl. Nano Mater.*, 2019, **2**, 6098–6102.

9 S. Moribe, Z. Chen, S. Alayoglu, Z. H. Syed, T. Islamoglu and O. K. Farha, *ACS Mater. Lett.*, 2019, **1**, 476–480.

10 Y. Zhang, X. Zhang, Z. Chen, K. Ichi Otake, G. W. Peterson, Y. Chen, X. Wang, L. R. Redfern, S. Goswami, P. Li, T. Islamoglu, B. Wang and O. K. Farha, *ChemSusChem*, 2020, **13**, 1710–1714.

11 D. W. Kim, D. W. Kang, M. Kang, J.-H. Lee, J. H. Choe, Y. S. Chae, D. S. Choi, H. Yun and C. S. Hong, *Angew. Chem., Int. Ed.*, 2020, **59**, 22531–22536.

12 E. Binaeian, Y. Li, H.-A. Tayebi and D. Yuan, *J. Hazard. Mater.*, 2021, **416**, 125933.

13 X. Han, W. Lu, Y. Chen, I. Silva, J. Li, L. Lin, W. Li, A. M. Sheveleva, H. G. W. Godfrey, Z. Lu, F. Tuna, E. J. L. Mcinnes, Y. Cheng, L. L. Daemen, L. J. M. McPherson, S. J. Teat, M. D. Frogley, S. Rudic, P. Manuel, A. J. Ramirez-cuesta, S. Yang and M. Schröder, *J. Am. Chem. Soc.*, 2021, **143**, 3153–3161.

14 C. Marsh, X. Han, J. Li, Z. Lu, S. P. Argent, I. da Silva, Y. Cheng, L. L. Daemen, A. J. Ramirez-Cuesta, S. P. Thompson, A. J. Blake, S. Yang and M. Schröder, *J. Am. Chem. Soc.*, 2021, **143**, 6586–6592.

15 M. K. Matikolaei and E. Binaeian, *ACS Appl. Mater. Interfaces*, 2021, **13**, 27159–27168.

16 L. Li, Y. Wang, J. Yang, Y. Chen and J. Li, *ChemPlusChem*, 2016, **81**, 222–228.

17 A. J. Rieth and M. Dinca, *J. Am. Chem. Soc.*, 2018, **140**, 3461–3466.

18 A. J. Rieth, Y. Tulchinsky and M. Dinca, *J. Am. Chem. Soc.*, 2016, **138**, 9401–9404.

19 K. Vikrant, V. Kumar, K.-H. Kim and D. Kukkar, *J. Mater. Chem. A*, 2017, **5**, 22877–22896.

20 B. Xiao, P. S. Wheatley, X. Zhao, A. J. Fletcher, S. Fox, A. G. Rossi, I. L. Megson, S. Bordiga, L. Regli, K. M. Thomas and R. E. Morris, *J. Am. Chem. Soc.*, 2007, **129**, 1203–1209.

21 G. W. Peterson, J. J. Mahle, J. B. DeCoste, W. O. Gordon and J. A. Rossin, *Angew. Chem., Int. Ed.*, 2016, **55**, 6235–6238.

22 X. Han, H. G. W. Godfrey, L. Briggs, A. J. Davies, Y. Cheng, L. L. Daemen, A. M. Sheveleva, F. Tuna, E. J. L. McInnes, J. Sun, C. Drathen, M. W. George, A. J. Ramirez-Cuesta, K. M. Thomas, S. Yang and M. Schröder, *Nat. Mater.*, 2018, **17**, 691–696.

23 J. Yang, B. Du, J. Liu, R. Krishna, F. Zhang, W. Zhou, Y. Wang, J. Li and B. Chen, *Chem. Commun.*, 2018, **54**, 14061–14064.

24 M. Savage, Y. Cheng, T. L. Easun, J. E. Eyley, S. P. Argent, M. R. Warren, W. Lewis, C. Murray, C. C. Tang, M. D. Frogley, R. T. Murden, M. J. Benham, A. N. Fitch, A. J. Blake, A. J. Ramirez-Cuesta, S. Yang and M. Schröder, *Adv. Mater.*, 2016, **28**, 8705–8711.

25 L. M. Rodriguez-Albelo, E. Lopez-Maya, S. Hamad, A. R. Ruiz-Salvador, S. Calero and J. A. Navarro, *Nat. Commun.*, 2017, **8**, 14457.

26 J. H. Carter, X. Han, F. Y. Moreau, I. Silva, A. Nevin, H. G. W. Godfrey, C. C. Tang, S. H. Yang and M. Schröder, *J. Am. Chem. Soc.*, 2018, **140**, 15564–15567.

27 J. B. DeCoste and G. W. Peterson, *Chem. Rev.*, 2014, **114**, 5695–5727.

28 N. S. Bobbitt, M. L. Mendonca, A. J. Howarth, T. Islamoglu, J. T. Hupp, O. K. Farha and R. Q. Snurr, *Chem. Soc. Rev.*, 2017, **46**, 3357–3385.

29 H. G. W. Godfrey, I. da Silva, L. Briggs, J. H. Carter, C. G. Morris, M. Savage, T. L. Easun, P. Manuel, C. A. Murray, C. C. Tang, M. D. Frogley, G. Cinque, S. Yang and M. Schröder, *Angew. Chem., Int. Ed.*, 2018, **57**, 14778–14781.

30 C. Petit and T. J. Bandosz, *Adv. Funct. Mater.*, 2010, **20**, 111–118.

31 J. Lee, C. Y. Chuah, J. Kim, Y. Kim, N. Ko, Y. Seo, K. Kim, T. H. Bae and E. Lee, *Angew. Chem., Int. Ed.*, 2018, **57**, 7869–7873.

32 J. G. Duan, W. Q. Jin and S. Kitagawa, *Coord. Chem. Rev.*, 2017, **332**, 48–74.

33 K. Wang, X.-L. Lv, D. Feng, J. Li, S. Chen, J. Sun, L. Song, Y. Xie, J.-R. Li and H.-C. Zhou, *J. Am. Chem. Soc.*, 2016, **138**, 914–919.

34 N. C. Burtch, H. Jasuja and K. S. Walton, *Chem. Rev.*, 2014, **114**, 10575–10612.

35 A. Yokozeki and M. B. Shiflett, *Appl. Energy*, 2007, **84**, 1258–1273.

36 A. Yokozeki and M. B. Shiflett, *Ind. Eng. Chem. Res.*, 2007, **46**, 1605–1610.

37 G. Li, Q. Zhou, X. Zhang, L. Wang, S. Zhang and J. Li, *Fluid Phase Equilib.*, 2010, **297**, 34–39.

38 K. N. Ruckart, Y. Zhang, W. M. Reichert, G. W. Peterson and T. G. Ind, *Ind. Eng. Chem. Res.*, 2016, **55**, 12191–12204.

39 T. Kajiwara, M. Higuchi, D. Watanabe, H. Higashimura, T. Yamada and H. Kitagawa, *Chem.–Eur. J.*, 2014, **20**, 15611–15617.

40 D. Saha and S. Deng, *J. Colloid Interface Sci.*, 2010, **348**, 615–620.

41 H. Furukawa, M. A. Miller and O. M. Yaghi, *J. Mater. Chem.*, 2007, **17**, 3197–3204.

42 K. J. Chang and O. Talu, *Appl. Therm. Eng.*, 1996, **16**, 359–374.

43 D. Ma, J. Zhang, J. Bai and H. Zhang, *Nat. Resour.*, 2014, **5**, 782–794.

44 J. A. Mason, M. Veenstra and J. R. Long, *Chem. Sci.*, 2014, **5**, 32–51.

45 S. Cha, M. Ao, W. Sung, B. Moon, B. Ahlstrom, P. Johansson, Y. Ouchi and D. Kim, *Phys. Chem. Chem. Phys.*, 2014, **16**, 9591–9601.

46 J. Joseph and E. D. Jemmis, *J. Am. Chem. Soc.*, 2007, **129**, 4620–4632.

47 O. V. Dolomanov, L. J. Bourhis, R. J. Gildea, J. A. K. Howard and H. Puschmann, *J. Appl. Crystallogr.*, 2009, **42**, 339–341.

48 G. M. Sheldrick, *Acta Crystallogr., Sect. A: Found. Adv.*, 2015, **71**, 3–8.

49 G. M. Sheldrick, *Acta Crystallogr., Sect. C: Struct. Chem.*, 2015, **71**, 3–8.

50 H. Furukawa, M. A. Miller and O. M. Yaghi, *J. Mater. Chem.*, 2007, **17**, 3197.

51 G. M. J. Frisch *et al.*, *Revision A.02*, Gaussian, Inc., Wallingford CT, 2009.

52 S. Dapprich, I. Komáromi, K. S. Byun, K. Morokuma and M. J. Frisch, *J. Mol. Struct.: THEOCHEM*, 1999, **461–462**, 1–21.

53 A. K. Rappe, C. J. Casewit, K. S. Colwell, W. A. Goddard and W. M. Skiff, *J. Am. Chem. Soc.*, 1992, **114**, 10024–10035.